EFDA–JET–PR(10)50

A.T. Salmi, T. Tala, G. Corrigan, C. Giroud, J. Ferreira, J. Lönnroth, P. Mantica,
V. Parail, M. Tsalas, T.W. Versloot, P.C. de Vries, K.-D. Zastrow
and JET EFDA contributors*

NBI Torque in Presence of Magnetic Field Ripple: Experiments and Modelling for JET

NBI Torque in Presence of Magnetic Field Ripple: Experiments and Modelling for JET

A.T. Salmi[1], T. Tala[2], G. Corrigan[3], C. Giroud[3], J. Ferreira[4], J. Lönnroth[1], P. Mantica[5], V. Parail[3], M. Tsalas[6], T.W. Versloot[6], P.C. de Vries[6], K.-D. Zastrow[3] and JET EFDA contributors*

JET-EFDA, Culham Science Centre, OX14 3DB, Abingdon, UK

[1] Aalto University, Association Euratom-Tekes, Helsinki, Finland
[2] VTT, Association Euratom-Tekes, Helsinki, Finland
[3] EURATOM/CCFE Fusion Association, Culham Science Centre, OX14 3DB, Abingdon, UK
[4] Associação EURATOM/IST, Centro de Fusão Nuclear, 1049-001 Lisbon, Portugal
[5] Istituto di Fisica del Plasma, EURATOM-ENEA-CNR Association, Milan, Italy
[6] FOM Institute Rijnhuizen, Association EURATOM-FOM, Nieuwegein, the Netherlands
** See annex of F. Romanelli et al, "Overview of JET Results", (23rd IAEA Fusion Energy Conference, Daejon, Republic of Korea (2010)).*

Preprint of Paper to be submitted for publication in
Plasma Physics and Controlled Fusion

ABSTRACT.
Accurate and validated tools for calculating toroidal momentum sources are necessary to make reliable predictions of toroidal rotation for current and future experiments. In this work we present the first experimental validation of torque profile calculation from neutral beam injection under toroidal field ripple. We use discharges from a dedicated experimental session on JET where neutral beam modulation technique is used together with time dependent torque calculations from ASCOT code for making the benchmark. Good agreement between simulations and experimental results is found.

1. INTRODUCTION

Toroidal momentum transport and rotation have been very active research topics during the last years. Toroidal rotation and rotation shear have been shown to improve confinement [1] and to increase the stability against resistive wall modes [2] of fusion plasmas. Recently it has been shown both theoretically [3,4] and experimentally [5–8] that inside the plasma pedestal momentum transport is not purely diffusive but that a convective (pinch) term also exists. Inward momentum pinch may help to achieve a peaked rotation profile in ITER even with the small external torque sources or with other seed rotation sources at the plasma edge [9].

One important ingredient in predicting rotation in ITER is the capability to calculate the torque generated by the NBI under toroidal magnetic field ripple. Even with the ripple compensating ferromagnetic inserts included in the design the expected ripple magnitude $\delta = (B_{max} - B_{min}) / (B_{max} + B_{min})$ in the full field will be $\delta \sim 0.35\%$ which, although shown to be acceptable in terms of fast ion energy losses [10], may still cause a significant counter current torque contribution via non-ambipolar radial diffusion of fast ions. In recent JET experiments [11] with enhanced ripple ($\delta \sim 1\%$) the plasma edge was found to counter rotate with co-current NBI while similar plasmas with smaller ripple were co-rotating. It was found that taking into account the NBI torque modification due to the ripple the observations could be largely explained. In Ohmic JET plasmas with ripple up to 1.5% non zero toroidal rotation has also been observed but the level of rotation has been small compared to NBI heated discharges [12].

Non-axisymmetric magnetic perturbations such as toroidal field ripple can also lead to non-ambipolar radial transport of thermal ions giving rise to the Neoclassical Toroidal Viscosity (NTV) torque, see e.g. a recent review [13] and references therein. Plasma breaking, associated with NTV, has indeed been observed experimentally on several tokamaks, e.g. DIII-D and JET using low toroidal harmonic magnetic perturbations. Toroidal field ripple, on the other hand, has a weak radial component which decays rapidly toward the plasma centre and the associated torque whether small or significant is expected to be edge localised. It is assumed that in the discharges analysed here NBI is the dominant *core* torque source and subsequently other possible torque sources such as the NTV or the residual stress [14] are neglected.

While ripple diffusion and trapping are well understood in theory, the rigorous validation of fast ion ripple torque calculations against experimental data are still lacking. In previous works e.g. [11,

15] from JET ripple campaign the ripple induced fast ion losses and torque have been identified as the likely candidate to explain the observed reduction in rotation. However, without detailed knowledge of the momentum transport in the discharges only rough estimates for the volume integrated total torque due to ripple can be obtained. For validating the torque calculations dedicated experiments are required in which both the diffusive and convective momentum transport (χ_ϕ and v_{pinch}) and the effect of ripple on NBI torque can be resolved simultaneously.

In this work, discharges from JET enhanced ripple session designed for benchmarking the NBI torque calculations in the presence of toroidal field ripple are analysed. The guiding centre following Monte Carlo code ASCOT [16] is used for the torque calculations. ASCOT has been used for fast ion loss calculations with ripple in, e.g. [17, 18] but has not yet been experimentally validated for the ripple torque.

The remainder of the paper is organised as follows. First the experimental set-up is described and the justification is given for the assumption of having an identical, Ion Temperature Gradient (ITG) dominated momentum transport between the discharges. This is followed by description of the plasma response to the applied NBI torque and power modulation. In Section 3 ASCOT code is first briefly described after which the ASCOT benchmark against OFMC [19, 20] and NUBEAM (inside the TRANSP transport code) [21] are presented. In Section 4 the ASCOT evaluated time dependent NBI torque profiles are reviewed and the experimental toroidal rotation measurements and their Fourier transformed amplitude, phase and steady state profiles are plotted and compared against torque calculations. Section 5 describes the optimisation scheme used to evaluate the momentum transport coefficients and presents the comparison between the simulated toroidal rotation, using NBI torque with ripple from ASCOT, and the experimental data. Finally, the results are discussed and conclusions of the work are drawn in Section 6.

2. EXPERIMENTAL SET-UP

The Neutral Beam Injection (NBI) system at JET [22] is well performing with a total of 16 units each delivering roughly 1-1.5MW of power and 1-1.5Nm of torque depending on the voltage and injection angle used. Half of the units are aligned with a tangency radius of $R_T = 1.31$m (normal injection) while the rest have a tangency radius of $R_T = 1.85$m (tangential injection) in the usual co-current direction. The major radius of the JET torus is $R_0 = 2.95$m. Their acceleration voltages can be adjusted from about 60kV to 130kV as required by the experiment. NBI power can also be turned on and off relatively reliably thus lending itself to transport studies utilising modulation techniques [23, 24].

A set of discharges were selected for this study (Pulse No's: 77089, 77090 and 77091) characterised by L-mode confinement and hence a relatively low density ($n_{e0} \approx 3\times10^{19}$ m^{-3}) and low temperature ($T_{e0} \approx T_{i0} \approx 3$keV), all with a plasma current of $I_p = 1.5$MA and the average central toroidal field $B_0 = 2.2$ T ($q_{95} = 5$). The three discharges did not exhibit MHD activity. In each discharge two 90keV NBI units (total of 2.5MW) are injected continuously to collect ion temperature and

toroidal rotation data and to keep that plasma relatively stationary during the experimental window. Additionally, two/three modulated 65keV units (≈4.5MW) are used with a duty cycle of 50/110 ms (on/off). The modulation cycle is short enough to avoid reaching steady state yet long enough to yield plasma rotation modulation sufficiently large to make the analysis. Pulse No: 77089 is the reference without ripple and with normal NBI modulation (3 units). Pulse No's: 77090 is identical to 77089 but operated with 1.5% toroidal field ripple (3 units). Pulse No: 77091 is again similar discharge with ripple and modulation from tangential NBI units (2 units).

Figure 1 shows time traces of a number of important plasma and heating parameters for Pulse No: 77089 with normal NBI modulation without ripple. The time interval shown is the same which is used for transport and torque analysis as well as for the Fourier analysis of the experimental profiles. One can observe that all the chosen quantities are modulated with the NBI except the thermal energy which within the experimental uncertainty shows no correlation with NBI power. This is consistent with the negligible density modulation that could be seen from the High Resolution Thompson Scattering (HRTS) diagnostics data (not plotted).

A more careful study, involving Fourier analysis, shows that in all discharges ion and electron temperature modulation are both between 2-5% of their steady state values while toroidal rotation modulation amplitude is significantly higher reaching up to 10% of the steady state. The small levels of the perturbations caused by the NBI modulation is the basis for our simplifying assumption that the momentum transport (χ_ϕ and v_{pinch}) is independent of the NBI power modulation and thus remains constant (in time) during the time interval of interest.

The similarity of the plasmas and equilibria across the discharges is illustrated in figure 2 which shows the experimental steady state profiles for the discharges 77089-77091. Ion and electron temperature profiles as well as the q-profiles are practically the same for all shots and the difference in electron density between the ripple and non-ripple reference discharges is below 10%. Based on the similar profiles among the three discharges we assume that the transport of momentum is the same between them and that the difference in the rotation is due to the difference in the torque source. This should be a reasonable assumption for ITG dominated turbulent transport since it mainly scales with ∇T_i [25] and they are identical.

In addition to the plasma properties also the location of the magnetic axis is modulated due to the NBI driven change in the plasma pressure. In fact the whole plasma moves rigidly without changing the shape. During the high power phase the plasma shifts around 1 cm towards the low field side. The equilibrium modulation combined with radial gradients in the profiles can generate spurious components in signals which are collected along fixed lines of sight. A simple estimation, using the 5mm radial modulation and the gradients involved shows that this could contribute about 5-20% to the modulation amplitudes if not subtracted in an appropriate way. In the following we eliminate the effect by mapping the data into time independent flux surface coordinates prior to the analyses.

3. CODE-TO-CODE BENCHMARKING

Multiple studies have been conducted to study the ripple effects, e.g. [26–28] giving analytical formulas and insights into the physical mechanisms. However, the analytical approach remains tricky for realistic simulations when complicated factors arise from e.g. toroidal field coil and NBI geometry, plasma shaping and from asymmetric fast ion distributions. These effects are, however, straightforwardly included in the orbit following Monte Carlo codes where also Coulomb collisions and their synergy with ripple are easily included. Nevertheless, it is useful, and helps to interpret the results later on, to see roughly what parameters are involved in ripple banana diffusion

$$\Delta = (N\pi / \sin\theta_t)^{1/2} (q\epsilon)^{3/2} \rho\delta \cdot \cos N\phi_t \quad [1]$$

Here Δ is the radial step size in ripple diffusion at the banana tip, N is the number of toroidal field coils, θ_t and ϕ_t are the poloidal and toroidal angles of the turning point, q is the safety factor, ϵ the inverse of the aspect ratio, ρ the gyro-radius of the ion and δ the ripple amplitude $\delta = (B_{max} - B_{min})/(B_{min} + B_{max})$. Even though this formula has been derived for circular plasmas with circular coils it shows that, since the diffusion coefficient $D = \Delta^2\tau^{-1}$ (τ = bounce time), under similar plasma conditions the diffusion is stronger for ions with higher energy and smaller pitch angle (=smaller θ_t) and in areas where the ripple is larger.

THE RIPPLE MODEL IN ASCOT

The ripple effect in guiding centre orbit following codes is included by tracing the ions in the 3D rippled magnetic field. For simulating JET plasmas with ASCOT we superimpose a sinusoidally varying toroidal magnetic field ripple on top of the axi-symmetric equilibrium field, B_0

$$B(r, z, \phi) = B_0(r, z) [1 + \delta_{16}(r, z) \cos 16\phi + \delta_{32}(r, z) \cos 32\phi] \quad [2]$$

Here, the axi-symmetric part is taken from EFIT. The numeric subscripts denote the 16th and 32nd toroidal harmonic of the Fourier decomposed vacuum ripple map. In normal JET operation all 32 toroidal field coils are driven with an equal amount of current which leads to very low ripple (0.08% at the separatrix on the outboard midplane). However, during enhanced ripple operation, where even and odd numbered toroidal field coils are driven with unequal currents δ_{16} becomes dominant since the ripple magnitude scales with the imbalance current roughly as $\delta_{16} \propto (I_{max} - I_{min})/(I_{min} + I_{max})$, where *min* and *max* denote the smaller and the larger of the currents in the odd and even numbered sets of coils.

Figure 3 shows the ripple contours ($\log_{10}\delta$) of the 16th Fourier harmonic amplitude. Ripple is largest at the outboard side of the plasma close to the midplane where it can reach levels up to 3.5%. In practice, to limit the heat loads, ripple magnitude is restricted to a maximum of ~ 1.5%. Ripple magnitude decays rapidly towards the core of the plasma and in practise inside the inner half of the plasma the ripple effect is negligible even at the highest allowed ripple.

4. ASCOT BENCHMARK AGAINST OFMC AND TRANSP

Before presenting our time dependent NBI torque evaluation for the NBI modulation under toroidal field ripple we compare ASCOT steady heat load calculations against those of the Orbit Following Monte Carlo code OFMC [10, 19]. OFMC has been developed and used extensively for JT-60U where it has been successfully benchmarked against experimental heat load data [29, 30]. More recently it has been used also for JET in preparation and analysis of JET ripple campaign analysis where a good quantitative agreement between the OFMC calculated heat loads due to fast ion losses and experimental values determined by the Infra Red camera were found [31].

Figure 4 shows an example of ASCOT calculation of the heat load on limiters and on the first wall on the low field side of the vacuum vessel. The main heat load from NBI is deposited on the poloidal limiters (grey bars) near the equatorial plane both with and without ripple. Heat load on limiters increases with ripple while at the same time localised heat loads below the mid-plane appear due to ripple trapping. This toroidally periodic heat load pattern, here around $\theta \sim -70$ deg, is due to the ripple trapped ions drifting vertically down from the high ripple region. The pattern and localisation of these heat loads are well suited for a code-to-code comparison of ripple losses. Both ASCOT and OFMC have been used extensively in the preparation and in the analysis of the JET ripple campaigns in 2006-2008 during which they have been cross checked against each other. Here we present one of the comparisons where both codes use a toroidally symmetric 2D limiter surface for clarity and statistics. We use EFIT equilibrium of the JET Pulse No: 60856 for making the benchmark together with the experimental temperature and density profiles. In this example we show data from simulations with artificially high ripple ($\delta \approx 3\%$) with 1MW of 130keV NBI. Both codes use their own model for the NBI geometry and for calculating the initial ionisation (birth profile).

One can see in the left frame of figure 5 that the codes predict nearly identical heat load patterns with the maximum loads deviating less than 10%. The toroidal angles $\phi = 0°$ and $\phi = 22.5°$correspond to the location of the high current coils, i.e. ripple minima and the dashed line at $\phi = 11.25°$correspond to the ripple well. Also, as expected, due to the 1/R dependence of the toroidal magnetic field, both codes show a slight shift of the maximum heat load from the ripple minimum in the co-current direction (here ϕ increases in counter current direction). The right frame shows a comparison of the energy distribution of the ions that cause the heat load on the limiter surface. At higher energies the curves are nearly identical. The deviation at lower energies is due to different lower energy thresholds in use for this comparison. Here ASCOT stops at higher average energy which naturally yields smaller losses at lower energies.

To validate ASCOT torque calculations without ripple it is compared against TRANSP for the non-ripple reference discharge (Pulse No: 77089). The calculated time dependent torque profiles from both codes are Fourier transformed at the 6.25Hz NBI modulation frequency and the resulting torque amplitude, phase and steady state profiles are compared in figure 6. The agreement between the codes is good with deviation of only about 10%. In previous work [24] ASCOT and TRANSP torques were additionally compared for collisional and $\mathbf{j} \times \mathbf{B}$ torque components with a good agreement.

5. EXPERIMENTAL DATA ANALYSIS

5.1. TORQUE EVALUATION

For calculating the NBI torque we use the experimental NBI power waveforms, acceleration voltages and fractions for the E, E/2 and E/3 energy components. For simplicity, since the plasma profiles are not significantly modulated by the NBI, we time average all the profiles and keep them constant during beam ionisation and slowing down calculations. We take the initial NBI ionisation profile from PENCIL [32] while the beam slowing down calculation and the ripple effect is accounted for with ASCOT.

Figure 7 summarises the result of torque evaluation for the three discharges. It shows the time traces of the volume integrated torque components and the time averaged torque densities for the modulated NBI units only. For better illustration only one NBI modulation cycle is pictured. The total torque is split to three components each with distinct time-scale: *collisional* torque due to Coulomb collisions, *instantaneous* torque which is essentially the toroidal component of the $\mathbf{j} \times \mathbf{B}$ force arising from the difference in the initial and bounce averaged flux surface of the ions. Thirdly, the *ripple* torque is due to the non-ambipolar radial diffusion of the NBI ions in the non-axisymmetric magnetic field. They all have different time scales and must be correctly resolved for simulating the inherently time dependent NBI modulation experiments.

As shown in figure 7, collisional torque is the slowest of the torque transfer mechanisms and takes place in about one collisional time (~150 ms). Instantaneous torque, like the name suggests, is almost instantaneous when compared to the usual slowing down time. Even in the absence of collisions it will take place in about one bounce time (~50μs) during which the initial bounce phases of the injected ions are randomised. Note that due to technical reasons in all the plots in this section the instantaneous torque further includes a small, and delayed, $\mathbf{j} \times \mathbf{B}$ torque component which arises when collisions (or ripple) move passing ions into trapped ones or vice versa. It is relatively easy to see that the time scale for the ripple torque must be somewhere between the $\mathbf{j} \times \mathbf{B}$ and collisional torques. This is because ripple diffusion only occurs at the tips of the trapped ion banana orbits and it necessarily takes several bounce times before any significant effect is accumulated. On the other hand, ripple diffusion scales with the fast ion energy (see Eq.1) making the effect faster than the collisional time. This is confirmed in the simulations which take into account these and other effects such as the injection angle (see figure 7). It is, furthermore, interesting to note that in the case of normal NBI modulation the fast ion ripple torque is stronger than the sum of the co-current torque components making the total modulated torque near the edge negative. In the tangential injection case the total torque is also considerably reduced due to the ripple but is only weakly negative at the edge.

Figure 8 clarifies the cause behind the differences in both the magnitude and the speed of response between the normal and tangential injections. The plot on the top left shows the initial turning point density together with a contour for ripple trapping boundary. This can be compared with figure 3 to see that with the normal injection the turning points locate in a region where the ripple amplitude is higher. The location of the turning points is governed by the pitch $\xi = v_{||}/v$ which for the tangential

case is larger (see top right frame). The bottom frames show that the difference in the trapped ion initial energy density is mainly due to the one less modulated NBI unit, not the trapping fraction which is the same for both. The difference in the injection power, however, is less than 1/3 while the difference in ripple torque (see figure 7) is a factor of 3 and can only partly explain the difference in the magnitude. The main cause for the difference in the magnitude of the ripple torques is the turning point location (=injection angle). The slower pace at which the ripple torque occurs with tangential injection is also due to the location of the turning points; while with normal injection the trapped ion turning points are instantaneously close to the maximum ripple level for a given flux surface, it will take a sizeable fraction of a collisional time before the pitch angle scattering has diffused the turning points of the tangentially injected trapped ions into the stronger ripple region. This will and add delay and reduce the magnitude of the ripple torque and is in line with the simulations. More details of the torque profiles are shown in the next section where they are Fourier transformed and plotted side-by-side with the corresponding experimental rotation profiles.

6. ROTATION MEASUREMENTS

The toroidal rotation of the plasma is measured with a Charge eXchange Recombination Spectroscopy (CXRS) diagnostic based on Carbon emission lines. The diagnostics has 12 horizontal lines of sight into the plasma which in this configuration cover the radius from the centre up to the pedestal top with a time resolution of 10ms and ±5% error in magnitude [33]. Based on earlier experiments on JET [34] and the weak temperature gradients in these discharges we expect that the bulk plasma (deuterium) rotation is nearly identical to that of the Carbon.

Figure 9 shows the toroidal angular frequency of the 3 discharges as a function of time for three modulation cycles within the analysis window. The greyed areas in the figures indicate the modulated NBI on time. From this data one can already qualitatively see the spin-up of the plasma when NBI is turned on. However, for Pulse No: 77090 with ripple, near the separatrix (lines at the bottom) the plasma actually accelerates in the opposite direction indicating that near the edge the ripple torque exceeds the co-current momentum from the NBI.

For a more quantitative analysis of the experimental rotation profiles we Fourier transform the data for all radial locations. The result at the 6.25 Hz NBI modulation frequency is shown in figure 10 (left column) where the rotation amplitudes, phases and the steady state profiles are plotted for the three discharges. For comparison the corresponding source terms from ASCOT, i.e. toroidal torque amplitude, phase and steady state are plotted adjacent on the right column.

The similarity of the experimental rotation amplitude and phase profiles and the correspondent calculated torque amplitude and phase profiles is striking. Note that information of rotation is not used in the torque calculation. This clearly indicates that the toroidal rotation is strongly influenced by the NBI torque. Even before the momentum transport analysis, the topic in the next section, one can see that the rotation profiles and their shapes seem to be consistent with the source profiles.

One of the most obvious differences between the discharges is the higher steady state rotation in

the non-ripple discharge (Pulse No: 77089) giving a clear indication of a large counter current torque in the rippled discharges. In Section it was found that ions from normal NBI experience stronger ripple effect than those from the tangential NBI. This is also clearly visible in the amplitude and phase plots for both the rotation and torque where the normal NBI with ripple (Pulse No: 77090) has larger and deeper penetrating amplitude than the one for the tangential NBI (Pulse No: 77091) even when accounting for the ~ 15% larger torque from 3 normal NBI units compared to 2 tangential units. The stronger ripple effect on normal NBI is also evident in the steady state profiles for rotation and torque. It is interesting to note that the radius of the minimum amplitude for the rotation and the torque for the normal NBI with ripple (Pulse No: 77090) coincide at $\rho_{tor} = 0.6$. This is, in fact, an important feature since it is found to improve the robustness of the torque validation by making the analysis less sensitive to the details of the toroidal momentum transport It may first seem odd that inside the mid radius where the ripple amplitude is negligible and where the torque profiles are identical for the normal NBI cases with (Pulse No: 77090) and without (Pulse No: 77089) ripple that there is a difference in the rotation phases. This feature, however, is well reproduced in the momentum transport analysis when both the pinch and the diffusion terms are included.

7. RIPPLE TORQUE VALIDATION

As already mentioned, no diagnostic exists that can measure the injected torque directly. CXRS diagnostics can measure the Carbon rotation but momentum transport analysis are required to relate the calculated torque source with the rotation. In our transport analysis we assume that for the non-ripple reference discharge the torque source is calculated accurately with ASCOT allowing us to use the NBI modulation technique to determine the momentum transport coefficients (χ_ϕ, v_{pinch}) without resorting to theoretical models or assumptions other than the momentum transport being independent of the NBI power modulation.

In this work we build on the scheme used in an earlier work [6,23,24,35,36] to find the optimal profiles for the Prandtl number, $Pr = \chi_\phi/\chi_i$, and the pinch velocity. Here we replace the manual trial and error profile optimisation with a non-linear minimising routine that allows simultaneous fitting of both pinch velocity and Prandtl number profiles. We also make an effort to set suitable optimisation criteria *a priori* and let the minimisation routine to find the *Pr* and v_{pinch} profiles that best reproduce the measured rotation profile in an automated way. Note that the fit is only done for the non-ripple discharge for which the torque calculations can be assumed to be accurate.

Similar to the previous work we use JETTO transport code to calculate the plasma response to the injected torque for given *Pr*, v_{pinch} profiles. We take the resulting time dependent rotation profile and Fourier transform it on all radii to obtain rotation amplitude and phase profiles at the NBI modulation frequency, and to get the steady state profile. The minimisation routine varies the *Pr*, v_{pinch} profiles until they produce the best possible match between the simulated rotation response and the experimental data for the amplitude, phase and steady state profiles simultaneously. As a figure of merit for the error in each profile we use the mean square error against the experimental

data which we normalise so that the error for the amplitude, phase and the steady state all yield roughly the same value near the optimum. The individual normalised errors are added together and the resulting error is the target of the minimisation.

Typically in one optimisation, with 5 radial points each for pinch and Prandtl number profiles, hundreds of transport simulations are needed for converged solution. To ensure the robustness in finding the global optimum in the multi dimensional parameter space we launch the above optimisation cycle several times, each with a randomly selected initial *Pr* and v_{pinch} profiles. Once repeated many times we usually find that most of the optimised profiles convergence to the same solution giving the assurance that the global optimum is found. During the optimisation the torque source is taken from ASCOT calculation.

In Figure 11 the result of the above optimisation cycle is shown for Pulse No: 77089. Black squares are the experimental data and the ensembles of red lines show the amplitude, phase and steady state profiles from all converged and nearly converged states where the total error is within 10% of the best fit. The dashed lines in the plots show the ±20% variation for the amplitude and the steady state and are there to help quantify the level of agreement achieved. The dashed line in the phase plot shows the ±11.25 deg variation corresponding to a 5ms time resolution. In the simulations we use 3-5ms resolution for the data while the time integration period for the rotation measurement is 10ms putting the 5ms as a reasonable estimate for the phase error. The bottom right frame in figure 11 shows the set of the pinch velocity and Prandtl number profiles that correspond to the described amplitude, phase and steady state profiles.

We find that roughly 30% variation in transport coefficients near the optimum is allowed while still giving a good fit against the experiment. There are a few reasons why this can be expected. Firstly, to some extent, small changes in the diffusion coefficient can be compensated by appropriate changes in the pinch velocity without increasing the total error significantly. Secondly, the definition of the total error (sum of mean squared errors) is not very sensitive to the profile shapes and can yield similar errors for qualitatively different profiles. Furthermore, as typical for profile optimisation, a small change in one profile point can partly be compensated by changes in the neighbouring points. However, even with the scatter in the profiles one can easily recognise the increasing trend towards the edge in both profiles which is consistent with the earlier work [6, 11].

The optimal profiles for the Prandlt number and the pinch velocity are shown in figure 12. We find that apart from the centre of the plasma the Prandtl number stays above unity in these L-mode discharges while slightly smaller values were previously found for the H-mode discharges [24] and in theory [37]. It is noteworthy also that for the first time on JET L-mode plasmas we find that non-zero pinch velocity is required to fit the rotation amplitude, phase and steady state profiles simultaneously.

The main piece of evidence in the experimental ASCOT NBI torque validation effort is shown in figure 13 where the comparison between the simulated toroidal rotation and the experimental measurements are plotted for each discharge. Note that the momentum transport is assumed to be

the same across all discharges as discussed earlier. It is seen that the simulated rotation response to the NBI modulation agrees well with the measurements. For all cases the time response (phase) is matched within about 11.25 deg corresponding to about 5 ms time resolution. Also the amplitude and steady state rotation profiles are well reproduced and largely stay within 20% of the experimental data. Furthermore, during the analysis it was seen that for the normal injection with ripple (Pulse No: 77090) the radius where the phase of simulated rotation changes its sign, $\rho_{tor} = 0.6$, is almost entirely determined by the torque source profile. When using Prandtl numbers that were smaller than the optimal found made the step too steep and accordingly Prandtl numbers larger than the optimum flattened the step while the radius where the sign reversal occurs remained nearly unaffected. These observations suggest that the NBI torque profiles with large ripple are consistent with measurements, a conclusion which is not very sensitive to the details of the momentum transport.

For completeness we used the optimisation scheme also for the discharges with ripple to see if the optimised transport would differ from the one obtained from the non-ripple reference case (see figure 12). We found that the agreement between the simulated and the measured rotation amplitude, phase and steady state profiles were only marginally improved compared to using the transport from the non-ripple discharge. This also implies that the momentum transport is indeed similar among the 3 discharges.

CONCLUSIONS

We have shown for the first time an experimental validation of a NBI torque profile calculation in the presence of large magnetic field ripple. We have used NBI modulation technique to deduce the prevalent momentum transport and time dependent torque calculations from ASCOT to make the comparison. We have developed a semi-automated way to analyse the transport in the NBI modulation experiments by building a scheme around a minimisation routine for getting a more comprehensive picture of the transport sensitivity. We have also validated ASCOT ripple operation numerically against OFMC by comparing heat load from ripple trapped ions and showed good agreement against TRANSP for the time dependent NBI torque evaluation without ripple. This work has shown that the guiding centre following Monte Carlo approach as used in ASCOT to calculate the NBI torque in presence of toroidal field ripple is accurate and can be used for predicting torque in conditions where the guiding centre approximation holds, such as ITER.

In this work we did no consider other torque sources besides the NBI. For the modulation part it can be well justified because the small induced plasma perturbations (δT_e, δT_i, δq, δn_e) are not expected to modify the ITG turbulence significantly. However, it is possible that some intrinsic sources were contributing to the steady state part. While they are mainly expected to be edge localised [37] experimental evidence for intrinsic core sources have also been reported [38]. In the transport optimisation we observed, similar to some earlier H-mode cases [6, 24], that for the best overall fit (simultaneous fit of the amplitude, phase and steady state rotation) the simulated rotation amplitudes tended to be slightly overestimated and the steady state rotation was underestimated.

While this on one hand could indicate a small error in the NBI torque calculations it may also point to an intrinsic core torque contribution like residual stress in co-current direction. It must be noted, however, because of the good agreement shown here, that the intrinsic core torque source in these discharges should be small.

For future work this method will be modified to allow systematic estimation of the magnitude of the intrinsic torque source in the core plasma even in the presence of NBI torque. For edge localised torque source studies this scheme would not seem to be as promising due to less accurate measurements in the pedestal region which makes it more difficult to separate the sources from the boundary contribution.

ACKNOWLEDGMENTS

Authors wish to thank Dr N. Oyama and Dr K. Shinohara for their help in setting up OFMC for JET. This work, supported by the European Communities under the contract of Association between EURATOM and Tekes, was carried out within the framework of the European Fusion Development. The views and opinions expressed herein do not necessarily reflect those of the European Commission.

REFERENCES

[1] H. Biglari, P. H. Diamond, and P. W. Terry. Influence of sheared poloidal rotation on edge turbulence. *Physics of Fluids B: Plasma Physics*, **2**(1):1–4, 1990.

[2] A.M. Garofalo, M.S. Chu, E.D. Fredrickson, M. Gryaznevich, T.H. Jensen, L.C. Johnson, R.J. La Haye, G.A. Navratil, M. Okabayashi, J.T. Scoville, E.J. Strait, A.D. Turnbull, and DIII-D Team. Resistive wall mode dynamics and active feedback control in diii-d. *Nuclear Fusion*, **41**(9):1171, 2001.

[3] A. G. Peeters, C. Angioni, and D. Strintzi. Toroidal momentum pinch velocity due to the coriolis drift effect on small scale instabilities in a toroidal plasma. *Physics Review Letters*, **98**(26):265003, Jun 2007.

[4] T. S. Hahm, P. H. Diamond, O. D. Gurcan, and G. Rewoldt. Nonlinear gyrokinetic theory of toroidal momentum pinch. *Physics of Plasmas*, **14**(7):072302, 2007.

[5] M. Yoshida, Y. Koide, H. Takenaga, H. Urano, N. Oyama, K. Kamiya, Y. Sakamoto, G. Matsunaga, Y. Kamada, and the JT-60 Team. Momentum transport and plasma rotation profile in toroidal direction in jt-60u l-mode plasmas. *Nuclear Fusion*, **47** (8):856, 2007.

[6] T. Tala, K.-D. Zastrow, J. Ferreira, P. Mantica, V. Naulin, A. G. Peeters, G. Tardini, M. Brix, G. Corrigan, C. Giroud, and D. Strintzi. Evidence of inward toroidal momentum convection in the jet tokamak. *Physics Review Letters*, **102** (7):075001, Feb 2009.

[7] W.M. Solomon, K.H. Burrell, A.M. Garofalo, A.J. Cole, R.V. Budny, J.S. deGrassie, W.W. Heidbrink, G.L. Jackson, M.J. Lanctot, R. Nazikian, H. Reimerdes, E.J. Strait, M.A. Van Zeeland, and the DIII-D Rotation Physics Task Force. Advances in understanding the generation and evolution of the toroidal rotation profile on diii-d. *Nuclear Fusion*, **49** (8):085005, 2009.

[8] P.C. de Vries, T.W. Versloot, A. Salmi, M-D. Hua, D. H. Howell, C. Giroud, V. Parail, G. Saibene, T. Tala, and JET EFDA Contributors. Momentum transport studies in jet h-mode discharges with an enhanced toroidal field ripple. *Plasma Physics and Controlled Fusion*, **52**(6):065004, 2010.

[9] T. Tala et al. Jet rotation experiments towards the capability to predict the toroidal rotation profile. *Proceedings of the 23rd International Conference on Fusion Energy, Daejong, Korea, 2010*, EXC/3-1, 2010.

[10] K. Shinohara, T. Oikawa, H. Urano, N. Oyama, and J. L˙ Effects of ferromagnetic components on energetic ion confinement in iter. *Fusion Engineering and Design,* 84(1):24 – 32, 2009.

[11] P.C. de Vries, A. Salmi, V. Parail, C. Giroud, Y. Andrew, T.M. Biewer, K. Crombé, I. Jenkins, T. Johnson, V. Kiptily, A. Loarte, J. Lönnroth, A. Meigs, N. Oyama, R. Sartori, G. Saibene, H. Urano, K.-D. Zastrow, and JET EFDA Contributors. Effect of toroidal field ripple on plasma rotation in jet. *Nuclear Fusion*, **48** (3):035007, 2008.

[12] M. F. F. Nave, T. Johnson, L.-G. Eriksson, K. Crombé, C. Giroud, M.-L. Mayoral, J. Ongena, A. Salmi, T. Tala, and M. Tsalas. Influence of magnetic field ripple on the intrinsic rotation of tokamak plasmas. *Physics Review Letters*, **105**(10):105005, Sep 2010.

[13] J.D. Callen. Effects of 3d magnetic perturbations on toroidal plasmas. *Proceedings of the 23rd International Conference on Fusion Energy, Daejong, Korea, 2010*, OV/4-3, 2010.

[14] P.H. Diamond, C.J. McDevitt, .D. Grcan, T.S. Hahm, W. X. Wang, E.S. Yoon, I. Holod, Z. Lin, V. Naulin, and R. Singh. Physics of non-diffusive turbulent transport of momentum and the origins of spontaneous rotation in tokamaks. *Nuclear Fusion*, **49**(4):045002, 2009.

[15] P. C. de Vries, E. Joffrin, N. C. Hawkes, X. Litaudon, C. D. Challis, Y. Andrew, M. Beurskens, M. Brix, J. Brzozowski, K. Crombé, C. Giroud, J. Hobirk, T. Johnson, J. Lönnroth, A. Salmi, T. Tala, V. Yavorskij, K-D. Zastrow, and JET EFDA Contributors. Effect of toroidal field ripple on the formation of internal transport barriers. *Plasma Physics and Controlled Fusion*, **50**(6):065008, 2008.

[16] J. A. Heikkinen and S. K. Sipilä. Power transfer and current generation of fast ions with large-k[sub theta] waves in tokamak plasmas. *Physics of Plasmas*, **2**(10):3724–3733, 1995.

[17] J.A. Heikkinen, W. Herrmann, and T.K. Kurki-Suonio. Fast response in the ripple trapped ion distribution to abrupt changes in a radial electric field in tokamaks. *Nuclear Fusion*, **38**(3):419, 1998.

[18] A. Salmi, T. Johnson, V. Parail, J. Heikkinen, V. Hynönen, T. P. Kiviniemi, T. Kurki-Suonio, and JET EFDA Contributors. Ascot modelling of ripple effects on toroidal torque. *Contributions to Plasma Physics*, **48**(1-3):77–81, 2008. CP:.

[19] K. Tani, M. Azumi, H. Kishimoto, and S. Tamura. Effect of toroidal field ripple on fast ion behavior in a tokamak. *Journal of the Physical Society of Japan*, **50**(5):1726–1737, 1981.

[20] K. Shinohara, H. Kawashima, K. Tsuzuki, K. Urata, M. Sato, H. Ogawa, K. Kamiya, H. Sasao, H. Kimura, S. Kasai, Y. Kusama, Y. Miura, K. Tobita, O. Naito, the JFT-2M Group, and D. S.

Darrow. Effects of complex magnetic ripple on fast ions in jft-2m ferritic insert experiments. *Nuclear Fusion*, **43**(7):586, 2003.

[21] A. Pankin, D. McCune, R. Andre, G. Bateman, and A. Kritz. The tokamak monte carlo fast ion module nubeam in the national transport code collaboration library. *Computer Physics Communications,* **159**(3):157 – 184, 2004.

[22] H. Altmann, H. Falter, A. Goede, R. Haange, R.S. Hemsworth, P. Kupschus, D. Stork, E. Thompson, G. Duesing. Neutral beam injection system. *Fusion Technology*, **11**(1):163–202, 1987. cited By (since 1996) 44.

[23] T. Tala, K. Crombé, P. C. de Vries, J. Ferreira, P. Mantica, A. G. Peeters, Y. Andrew, R. Budny, G. Corrigan, A. Eriksson, X. Garbet, C. Giroud, M-D. Hua, H. Nordman, V. Naulin, M. F. F. Nave, V. Parail, K. Rantamki, B. D. Scott, P. Strand, G. Tardini, A. Thyagaraja, J. Weiland, K-D. Zastrow, and JET-EFDA Contributors. Toroidal and poloidal momentum transport studies in tokamaks. *Plasma Physics and Controlled Fusion*, **49**(12B):B291, 2007.

[24] P. Mantica, T. Tala, J. S. Ferreira, A. G. Peeters, A. Salmi, D. Strintzi, J. Weiland, M. Brix, C. Giroud, G. Corrigan, V. Naulin, G. Tardini, K.-D. Zastrow, and JET-EFDA Contributors. Perturbative studies of toroidal momentum transport using neutral beam injection modulation in the joint european torus: Experimental results, analysis methodology, and first principles modeling. *Physics of Plasmas*, **17**(9):092505, 2010.

[25] W. X. Wang, P. H. Diamond, T. S. Hahm, S. Ethier, G. Rewoldt, and W. M. Tang. Nonlinear flow generation by electrostatic turbulence in tokamaks. *Physics of Plasmas*, **17**(7):072511, 2010.

[26] R. J. Goldston, R. B. White, and A. H. Boozer. Confinement of high-energy trapped particles in tokamaks. *Physics Review Letters*, **47**(9):647–649, Aug 1981.

[27] P. N. Yushmanov. *Reviews of plasma physics*, **16**:117, 1990.

[28] V Ya Goloborod'ko, Ya I Kolesnichenko, and V A Yavorskij. Alpha particle transport processes in tokamaks. *Physica Scripta*, **1987**(T16):46, 1987.

[29] Y. Ikeda, K. Tobita, K. Hamamatsu, K. Ushigusa, O. Naito, and H. Kimura. Ripple enhanced banana drift loss at the outboard wall during icrf/nbi heating in jt-60 u. *Nuclear Fusion*, **36**(6):759, 1996.

[30] K. Tobita, K. Tani, Y. Neyatani, A. A. E. van Blokland, S. Miura, T. Fujita, H. Takeuchi, T. Nishitani, M. Matsuoka, and S. Takechi. Ripple-trapped loss of neutral-beam-injected fast ions in JT-60u. Physics Review Letters, **69**(21):3060–3063, Nov 1992.

[31] T. Johnson, J. Lönnroth, P.C. de Vries, A. Salmi, L.-G. Eriksson, J. Ongena and N. Oyama and V. Parail and G. Saibene and S. Sharapov V. Hynönen, and I. Jenkins, K. Shinohara, and JET-EFDA contributors. Halekar modelling of fast particle transport and losses with tf ripple in jet. *In 10th IAEA Technical Meeting on Energetic Particles in Magnetic Confinement Systems*.

[32] C.D. Challis et al. *Nuclear Fusion*, **29**:563, 1989.

[33] Carine Giroud, A. G. Meigs, C. R. Negus, K.-D. Zastrow, T. M. Biewer, T. W. Versloot, and

JET-EFDA Contributors. Impact of calibration technique on measurement accuracy for the jet core charge-exchange system. *Review of Scientific Instruments*, **79**(10):10F525, 2008.

[34] D. Testa, C. Giroud, A. Fasoli, K.-D. Zastrow, and EFDA-JET Team. On the measurement of toroidal rotation for the impurity and the main ion species on the joint european torus. *Physics of Plasmas*, **9**(1):243–250, 2002.

[35] P. Mantica, D. Strintzi, T. Tala, C. Giroud, T. Johnson, H. Leggate, E. Lerche, T. Loarer, A. G. Peeters, A. Salmi, S. Sharapov, D. Van Eester, P. C. de Vries, L. Zabeo, and K.-D. Zastrow. Experimental study of the ion critical-gradient length and stiffness level and the impact of rotation in the jet tokamak. *Physics Review Letters*, **102**(17):175002, Apr 2009.

[36] G. Tardini, J. Ferreira, P. Mantica, A.G. Peeters, T. Tala, K.D. Zastrow, M. Brix, C. Giroud, G.V. Pereverzev, and JET-EFDA contributors. Angular momentum studies with nbi modulation in Jet. *Nuclear Fusion*, **49**(8):085010, 2009.

[37] A. Peeters et al. Toroidal momentum transport. *Proceedings of the 23rd International Conference on Fusion Energy, Daejong, Korea, 2010,* OV/5-4, 2010.

[38] W. M. Solomon, K.H. Burrell, A.M. Garofalo, S.M. Kaye, R.E. Bell, A.J. Cole, J.S. de Grassie, P.H. Diamond, T.S. Hahm, G.L. Jackson, M.J. Lanctot, C.C. Petty, H. Reimerdes, S. A. Sabbagh, E.J. Strait, T. Tala, and R.E. Waltz. Mechanisms for generating toroidal rotation in tokamaks without external momentum input. *Physics of Plasmas*, **17**(5):056108, 2010.

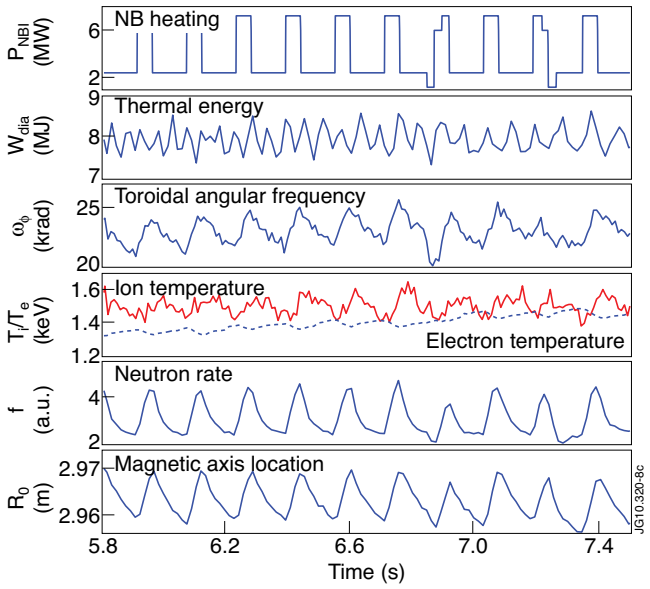

Figure 1: Time traces of plasma and heating parameters over the time interval of interest for Pulse No: 77089. Temperature and rotation values are taken near plasma mid radius and magnetic axis from EFIT reconstruction.

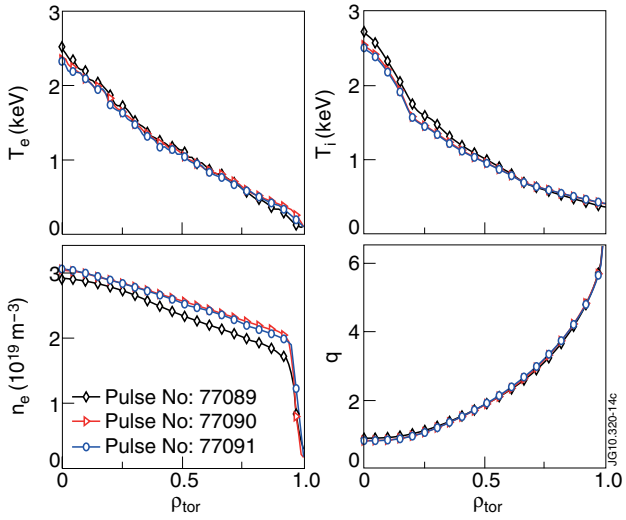

Figure 2: Time averaged plasma and q-profiles over 9 modulation cycles between 6.0s – 7.44s for the Pulse No's: 77089 (diamond), 77090 (triangle) and between 7.0s – 8.44s for Pulse No: 77091 (circle).

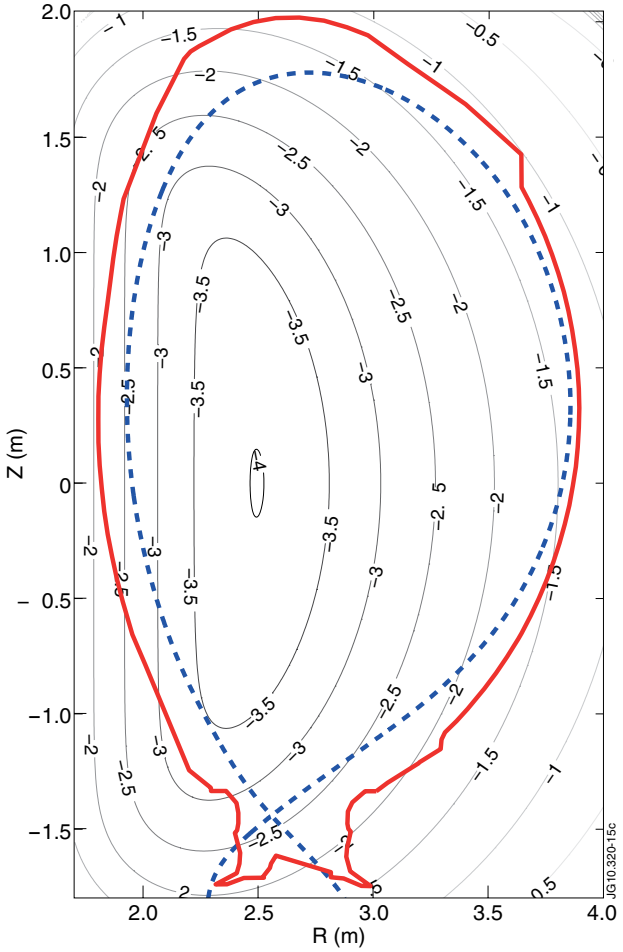

Figure 3: Ripple map for JET 16 coil harmonic together with the cross section of the limiter surface and a seperatrix for a typical equilibriam. Number on the contours give the log_{10} of the ripple amplitude.

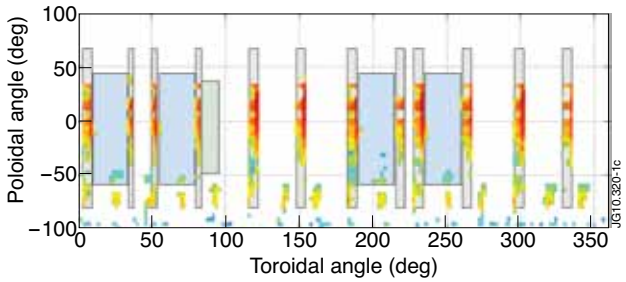

Figure 4: 2D projection of the heat load on the first wall and limiters from NBI in JET under 1.5% ripple as calculated by ASCOT. Blue rectangles show the RF and LH antennas and grey elongated structures the polodial limiters designed to withstand heat loads up to several MWm^{-2}.

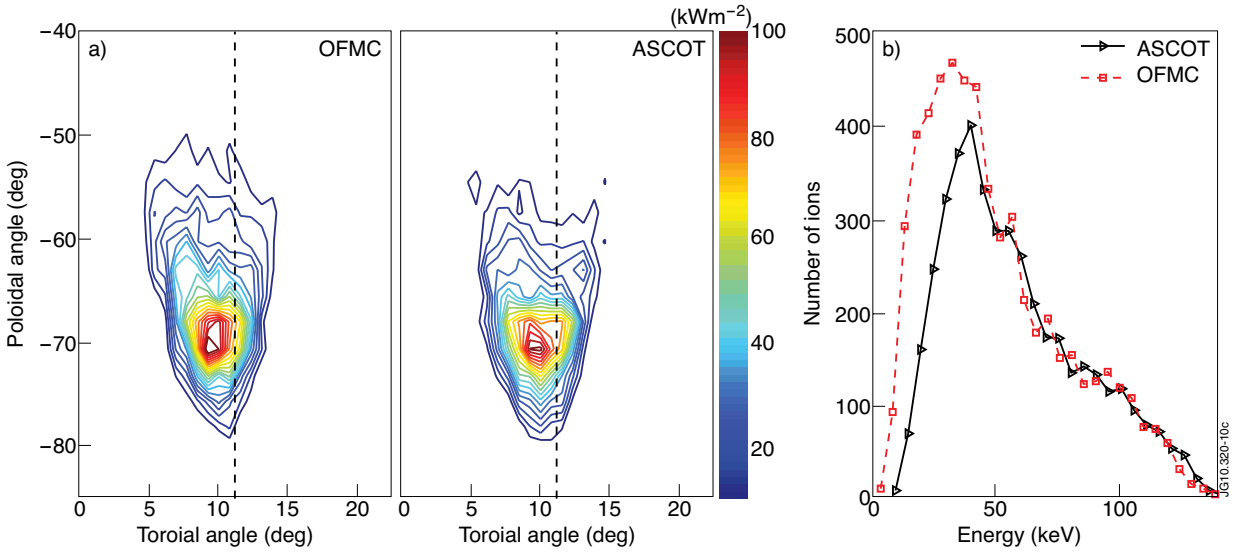

Figure 5: a) Heat load from the ripple trapped ions in the ripple well region as calculated by OFMC and ASCOT. Dashed line shows the toroidal location of ripple minimum. b) Energy spectra of the ripple trapped losses.

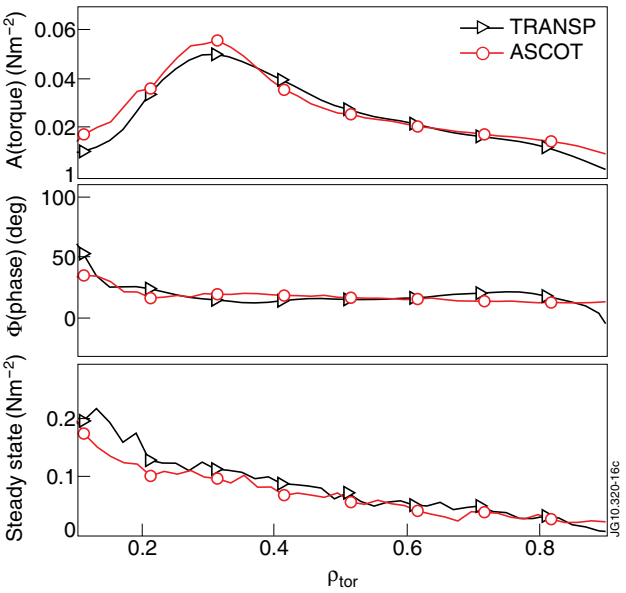

Figure 6: Comparisopn of ASCOT and TRANSP torque evaluation for the non-ripple discharge (Pulse No: 77089). Frames from the top show: the Fourier amplitude profile at the 6.25Hz modulation frequency, the Fourier phase with respect to the NBI power, and the steady state torque transfer.

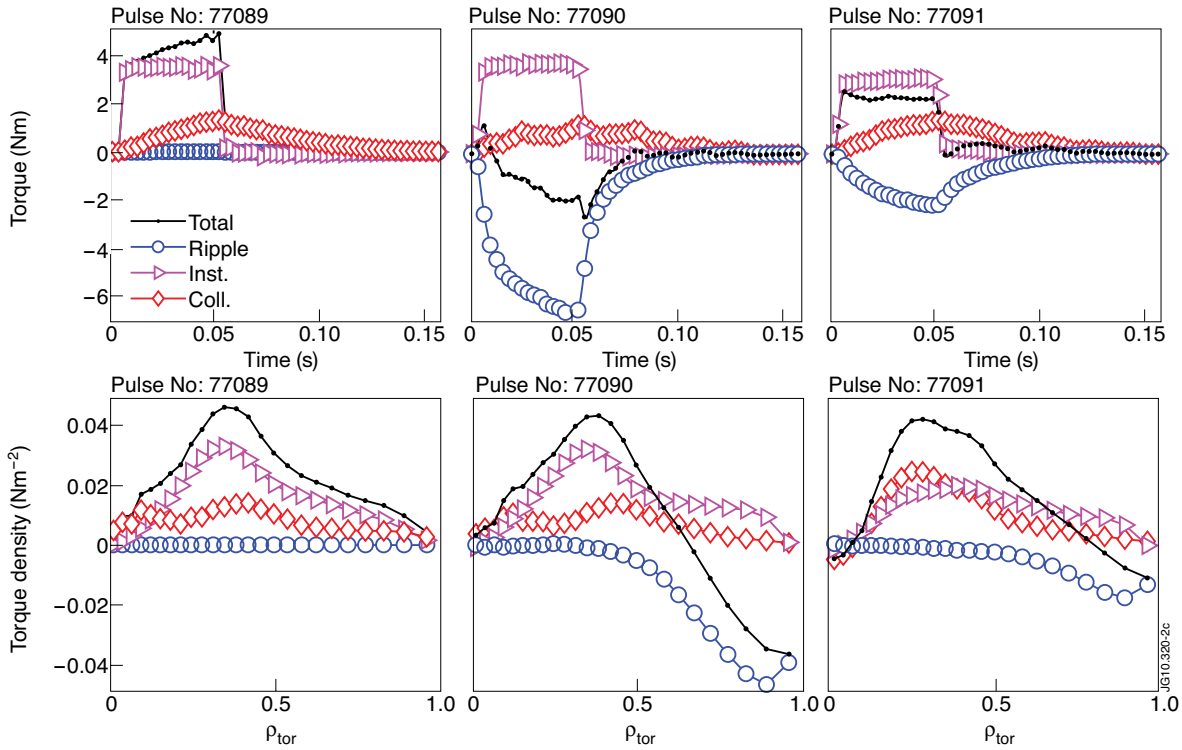

Figure 7: One modulation cyle data for the modulated NBI units only. Top row shows the volume integrated torque seperated in ripple, collisional and instantaneous componenst. Bottom row shows cyle averaged torque densities for each component. Note that Pulse No: 77091 only has two modulated NBI units.

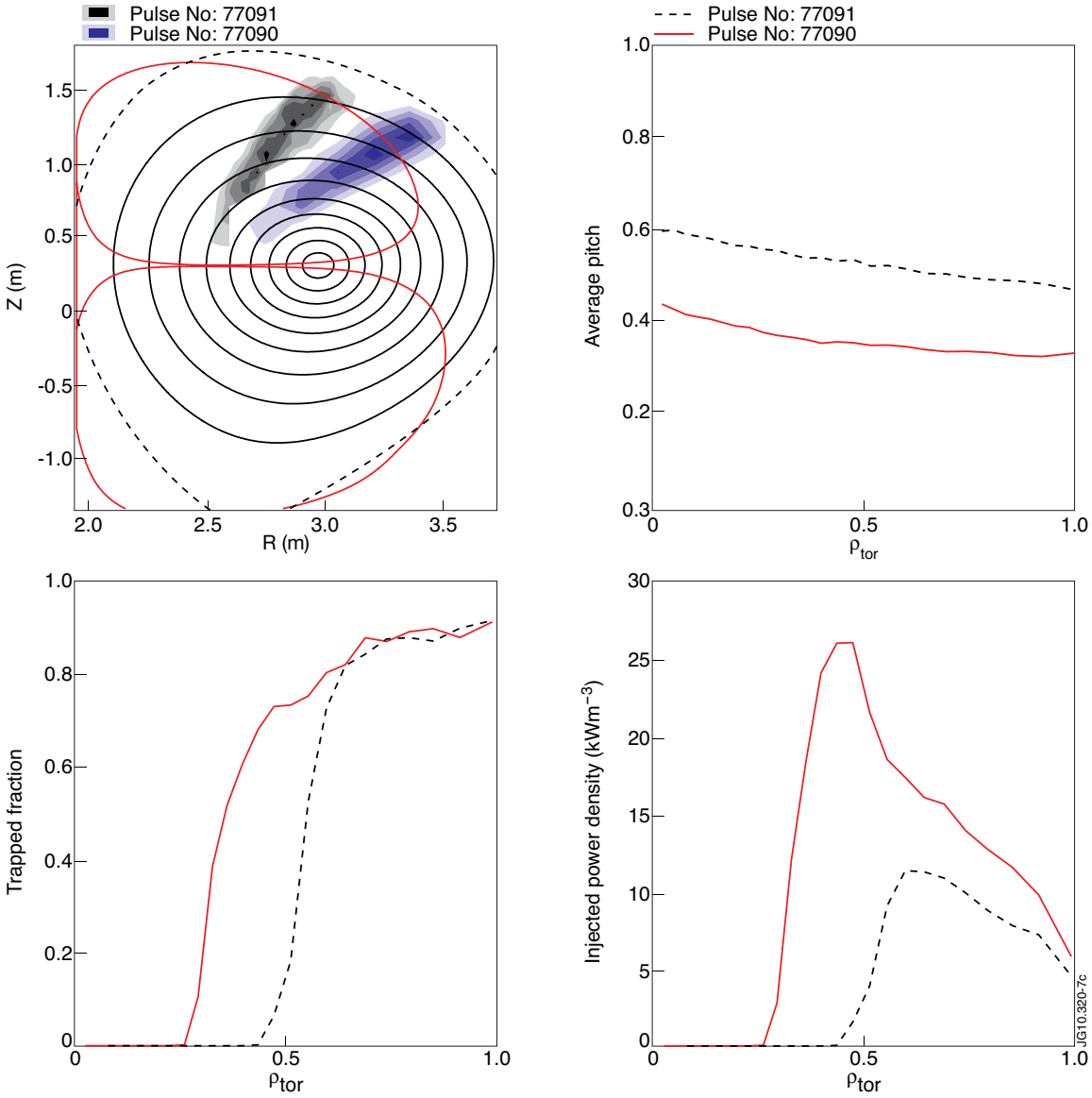

Figure 8: Initial NBI characteristics for trapped ions. a) turning point density on polodial cross section for normal (Pulse No: 77090) and tangential (Pulse No: 77091) injection. The red lines confine a ripple well free region. b) the average initial pitch of all NBI ions, c) the fraction of trapped ions and d) the injected energy density of trapped ions.

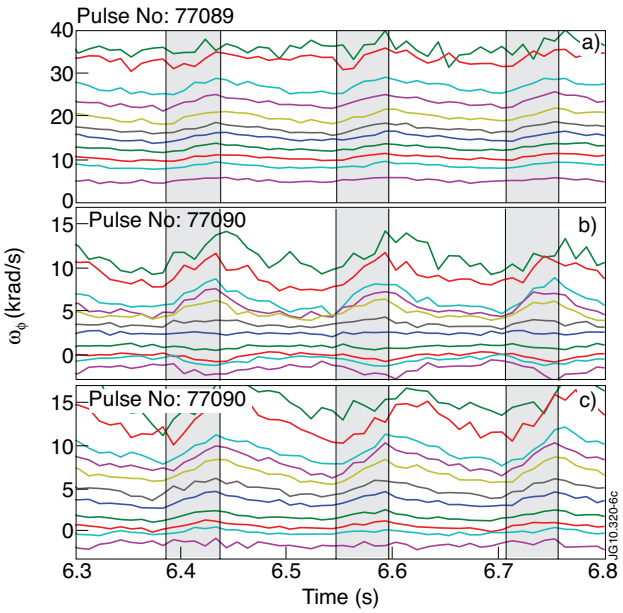

Figure 9: Time traces of CX measurements of toroidal angular frequency at various lines of sight for a) normal NBI without ripple (Pulse No: 77089) b) normal NBI with ripple (77090) and c) tangential NBI with ripple (Pulse No: 77091). Gray bars indicate the time when modulated NBI is on. Due to the monotonic rotation profile (see figure 2) high values correspond to the centre (R=3.05m) and low values to the edge of the plasma (R=3.78m).

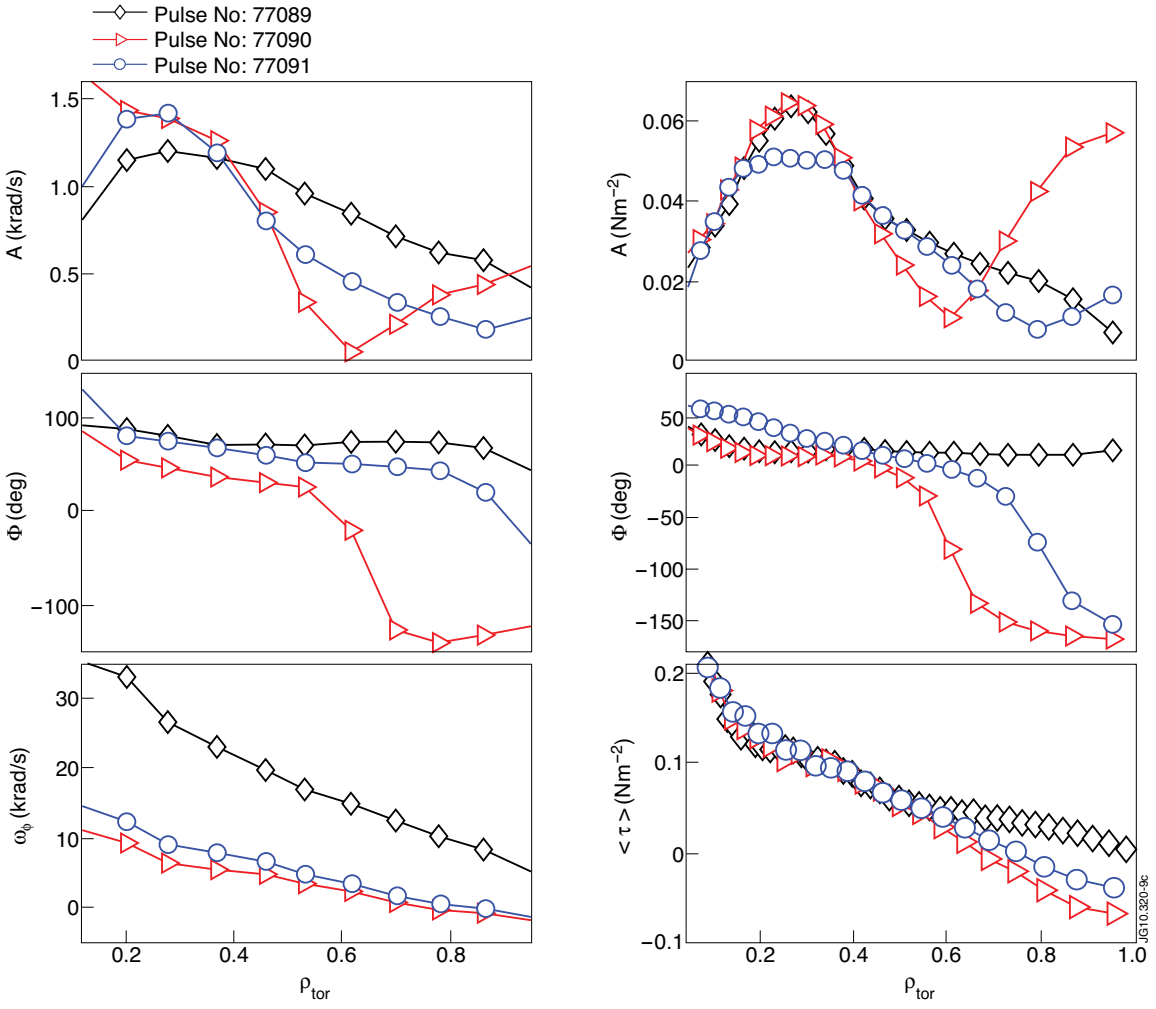

Figure 10: Fourier amplitudes (top), phases (middle) and steady state values (bottom) of the experimental toroidal rotation profiles (left column) and calculated torque profiles (right column).

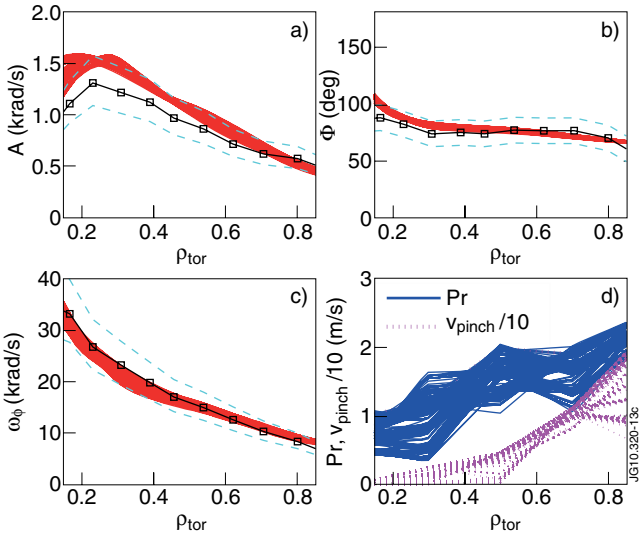

Figure 11: Ensemble of red lines give the rotation a) amplitude b) phase c) steady state of the simulations that yeild a target error that is within 10% of the best fit. The corresponding Prandtl number and pinch velocity profiles are plotted in the lower right frame. Black lines with square markers show the experimental data and the dashed lines give the 20% interval around the measurements for rotation and rotation amplitude and 11.25 deg (5ms equivalent in time) for phase and help to quantify the quality of the fit.

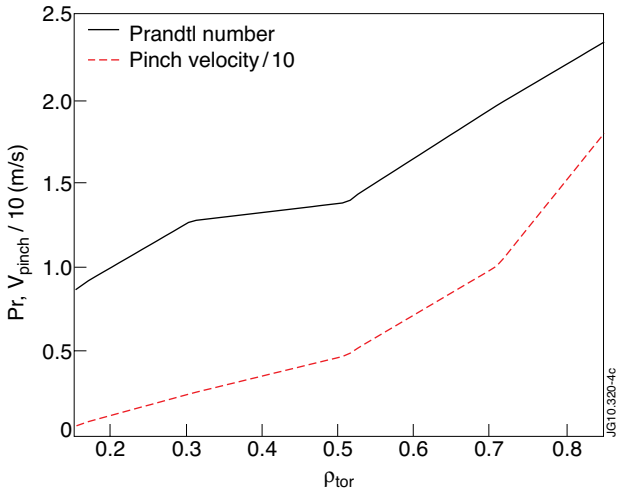

Figure 12: Optimised Prandtl number and pinch velocity profiles for Pulse No: 77089.

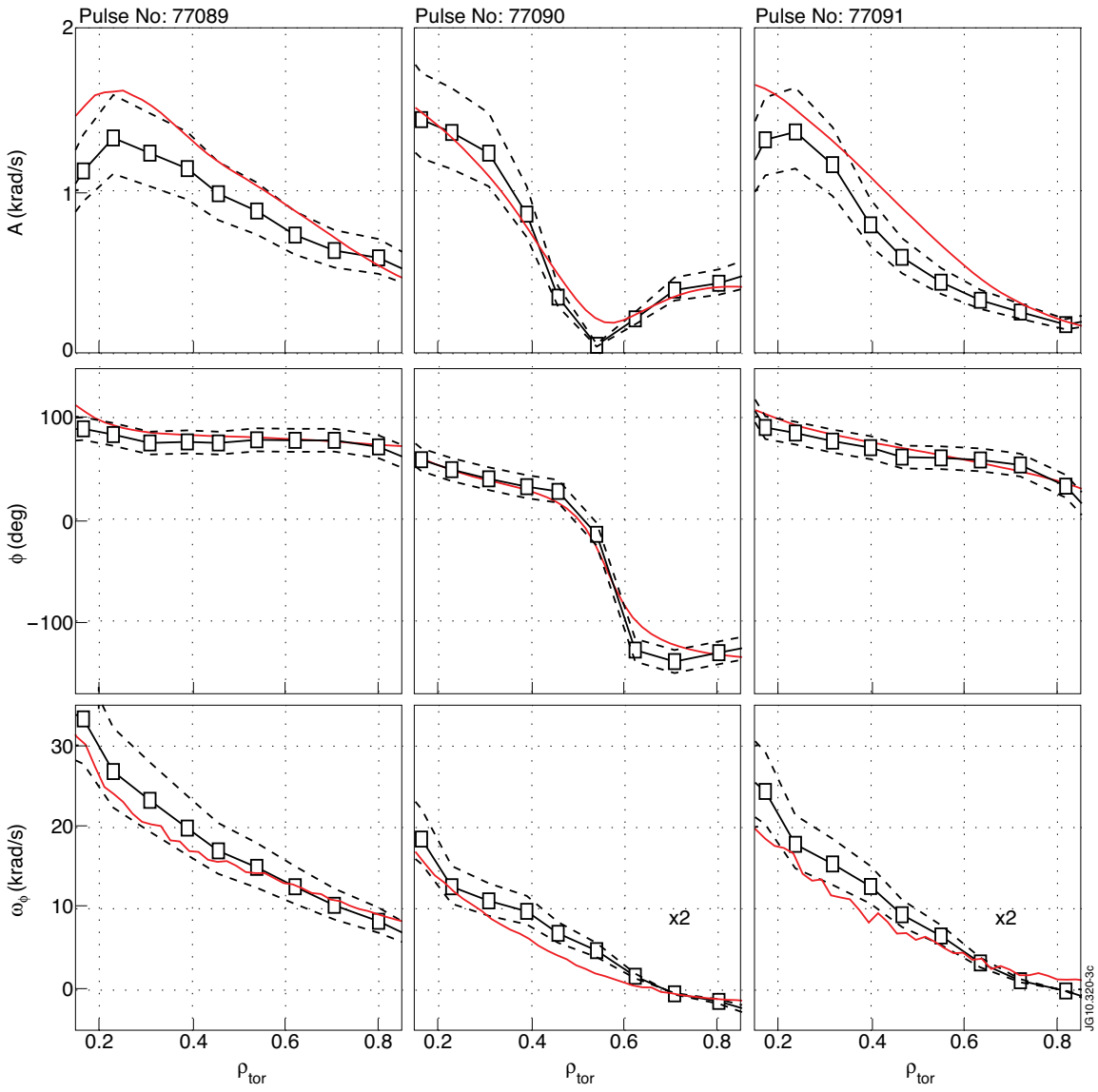

Figure 13: Amplitude, phase and steady state profiles for the three discharges using the optimised Prandtl number and pinch velocity profiles for Pulse No: 77089 (see figure 12). First column correspond to the Pulse No: 77089, second column to Pulse No: 77090 and third coloumn to Pulse No: 77091. Dashed lines are to guide the eye and give rough estimates of the error.